UNIVERSITY OF CALIFORNIA,
IRVINE

Optical Oxygen Sensing in the Murine Subcutaneous Space for Islet Transplantation

THESIS

submitted in partial satisfaction of the requirements
for the degree of

MASTER OF SCIENCE

in Biomedical Engineering

by

Mellonie Zhang

Thesis Committee:
Professor Elliot L. Botvinick, Chair
Professor Bernard Choi
Associate Professor Wendy Liu

2019

DEDICATION

To

My sister
May you always be curious to learn and explore.

My father
Thank you for always encouraging me to push myself for the better and the greater.

And especially, my mother
Thank you for always believing in me even when I feel like giving up. I would not be the person I am today without you.

"*The important thing is to not stop questioning. Curiosity has its own reason for existing.*"
- Albert Einstein

"I'm still learning."
- Michelangelo

TABLE OF CONTENTS

LIST OF FIGURES

ACKNOWLEDGMENTS

I would like to express the deepest appreciation to my committee chair, Professor Elliot Botvinick. He has been an amazing mentor who has encouraged and supported me through both the highs and lows of graduate school. His kindness and mild-temperament are astonishing, and his ability to dissolve complex or tense situations with humor is admirable. When I first met Elliot, I knew nothing about engineering. He has always patiently taught me and cheered me on even for my smallest accomplishments. His passion for science is contagious and energizing. Elliot always tries to make himself available for his students and tries his best to help us whenever he can. He continues to inspire me to grow both as a scientist and an individual.

I would also like to thank my committee members, Professor Bernard Choi and Professor Wendy Liu, whose advice and suggestions throughout this process have been insightful and incredibly helpful.

In addition, I would like to thank my fellow lab members, who had all contributed to this work in one way or another. Their friendships have made my two years at UCI an experience I will never forget. I would especially like to thank Dr. John Weidling, Dr. Mark Keating, Dr. Avid Najdahmadi, and Rachel Gurlin, for their patient guidance and persistent help. Without them, this thesis would not have been possible.

Thank you also to my boyfriend, Andrew Phan. He has been my rock through all of this.

Finally, thank you to my family. Without their support, I would not be here today. Thank you to my parents who immigrated to the US to provide their children with a better future and new opportunities that they did not have themselves. Thank you for always supporting me and loving me despite life's ups and downs. They have moved my sister and I all around the world to make sure we get the best education and most comfortable life. Especially, thank you to my mother who has always talked to me and encouraged me like a friend. She inspires me every day and is my biggest role model. Thank you to my sister for looking up to me and motivating me to work harder and achieve greater. I love you all.

Thank you to JDRF for providing the financial support for this work.

ABSTRACT OF THE THESIS

Optical Oxygen Sensing in the Murine Subcutaneous Space
for Islet Transplantation

By

Mellonie Zhang

Master of Science in Biomedical Engineering

University of California, Irvine, 2019

Professor Elliot L. Botvinick, Chair

Type 1 diabetes (T1D) is an autoimmune disease that affects 1.25 million Americans. Although there have been many technological advancements that improve the care and maintenance of the disease, there is currently still no cure. Transplanting islets of Langerhans has shown potential to maintain normoglycemia in patients, and to prolong the effects of this cell therapy, tissue engineering devices have been used to protect the cells from the host's immune response. However, the mass transport of oxygen and nutrients in these devices for islet survival and insulin secretion has been limited due to the long distances between cells and the host's vasculature system and slow diffusion rates. Pre-vascularization of the scaffold is a process in which the scaffold is implanted and allowed to vascularize before the cells are transplanted. This may improve success of the implant by providing a closer source of metabolic transport for the cells.

In the first chapter, we demonstrated a technique to optically measure oxygen concentrations non-invasively in subcutaneously implanted PDMS-based tissue scaffolds over eight weeks. Tracking oxygen diffusion rates at the site of implantation over time may

provide insight into the vascularization process and the optimal time for pre-vascularization. To further increase reliability of the oxygen measurements, in the second chapter, an optical oxygen sensor is developed that uses the phase shift between the sinusoidally modulated excitation and emission signals. Fewer sampling points are needed to accurately characterize a wave function than an exponential function, which yields more robust and reliable measurements.

Chapter 1: Introduction

1.1 Type 1 Diabetes

Type 1 diabetes (T1D) is a chronic autoimmune disease that affects 1.25 million Americans, with the number expected to grow to 5 million by 2050.[1,2] Approximately $14 billion is spent each year on related healthcare and lost labor costs.[1] In T1D, the immune system attacks pancreatic beta cell clusters, known as islets, resulting in an inability to produce insulin, a hormone that regulates the uptake of blood glucose into cells.[3] Patients rely on daily injections of exogenous insulin to control blood glucose levels; however, less than one-third of patients are able to consistently maintain their A1C within the American Diabetes Association target ranges.[3,4] Managing blood glucose is also complicated by factors, such as age, gender, race, diet, exercise or general health, which may influence the amount of insulin the patient needs.[5] Mis-regulation of blood glucose can cause both hyperglycemia and hypoglycemia, which, especially over extended periods of time, could lead to severe organ damage over time or death.[1,3]

Other than needing to be constantly vigilant about their blood glucose levels, T1D affects many other aspects of patients' lives. Both sleep and exercise are necessary to improve blood glucose control but are often negatively impacted by the disease.[6,7] Studies have shown that patients with T1D spend more time in light sleep than in deep sleep when compared to their healthy counterparts, which causes elevated A1C levels.[6] Furthermore, many patients experience irregular blood glucose patterns after exercise, which makes it difficult to predict the appropriate dosage of insulin needed.[7] This may have fatal consequences, in particular hypoglycemia, that could cause patients to be wary and reluctant to exercise.[7] The lack of

sleep and exercise that is caused by T1D drives a negative feedback loop that further worsens patient health and complicates blood glucose and disease management over time. Therefore, it is critical to have effective treatments that could prevent, or even reverse, disease progression and complications.

1.2 Standard Care

Traditionally, blood glucose levels are monitored and controlled by daily finger pricks along with insulin injections via a syringe. Patients typically need at least six finger pricks a day to track and predict their blood glucose and administer the appropriate amounts of insulin.[8,9] However, this method does not provide effective glucose control due to large fluctuations throughout the day between readings and inaccurate insulin predictions.[8–10] The development of insulin pumps offered increased glucose control and reduced the number of needle punctures patients need.[9,10] The insulin pump is connected to the body via an infusion set and continuously delivers insulin based on each patient's basal rate and inputted food consumptions.[10] Additionally, continuous glucose monitors (CGMs) allow for further control by continuously tracking patient blood glucose via a small sensor under the skin, which allows for better diabetes management.[9,11] However, despite these innovations, the majority of T1D patients still do not have their A1C within target ranges since many other biological factors and cues that may influence blood glucose patterns are not accounted for in these systems.[4,9] More effective devices, techniques, and therapies are needed for patients to have optimal metabolic control.[9]

Pancreas transplants have also been considered as a treatment method in small amounts of T1D patients. Pancreas transplants are usually only performed in severe cases where the patient also has end-stage renal failure or have life-threatening hypoglycemia unawareness

due to limited by the number of available organs and high risks.[12–14] The pancreas transplant surgery is a major procedure that poses significant risks, such as infections, organ rejection, and higher morbidity and mortality rates than other transplants, that may outweigh the benefits.[13,14] Although patients are able to maintain normoglycemia without constant blood glucose monitoring and insulin injections, they have to rely on daily administration of immunosuppressants, which can still be tedious and puts the risk patient at risk of immune-related complication.[13,14] Therefore, a solution that can relieve patient dependency on insulin without the high associated risks is needed.

Although there have been many technological and medical advances that increase the effectiveness of diabetes care and management, there is currently still no widespread and easily-accessible cure for T1D. Patients still have to use multiple cumbersome devices or develop lifetime dependency on immunosuppressants. Tissue engineering with pancreatic islets have shown potential as a cure for T1D that would allow patients to regain endogenous insulin secretion and blood glucose monitoring functions with less health risks than whole organ transplants.[15]

1.3 Tissue Engineering Approaches

Tissue engineering has been an emerging field since the early 1990s as a plausible method to restore or replace damaged tissue or organs.[16] In the case of T1D, it has been shown that transplantation of the islets of Langerhans, which contain endocrine cells, could restore endogenous insulin secretion and glucose homeostasis functions.[17] To prolong the effects of this cell therapy, tissue engineering devices have been used. One of the greatest challenges of successful tissue engineering is protecting the implanted cells from the host's immune response, while still allowing adequate delivery of oxygen and nutrients for cell

survival.[18] Encapsulation methods, such as with alginate microbeads, completely encase the transplanted islets and prevent them from being destroyed by macrophages.[18] However, these capsules cut the islets off from any access to vital resources.[18] In order to have efficient delivery of oxygen and nutrients, blood vessels should be located within close proximity of the transplanted islets.[19] Various porous materials have been used to promote angiogenesis and allow vessels to infiltrate, thereby reducing the distance resources have to diffuse across.[19] The material and geometry properties of the tissue scaffold also mediate the interactions between the scaffold, transplanted cells, and blood elements.[20] The permeability of the scaffold material directly correlates with the diffusion rate of oxygen from the vasculature to the cells, and materials with high oxygen permeability, such as PDMS, are desirable.[21,22] Certain materials, such as polystyrene, and rougher scaffold surfaces have been shown to recruit and promote the activation of monocytes and macrophages, which cause the formation of fibrotic capsules.[19,20] This limits the vascularization of the implant and restricts the cell from accessing oxygen and nutrients.[20]

Lack of oxygen can cause cell apoptosis and necrosis, and ultimately result in the failure of the implant.[23] While currently there are many techniques to measure oxygen levels *in vivo*, there is no method that is able to localize the measurements to the exact islet implantation sites. Oxygen is normally only quantified at the general area of implantation via various invasive and noninvasive methods, rather than the exact scaffold-cell interface.[24] Oxygen diffusion through a scaffold can be impacted by its material properties, so regions of implantation with high levels of oxygenation do not ensure that adequate amounts of oxygen are actually reaching the implanted cells.[21] Pre-vascularization of the scaffold is a possible approach to improve the success of the implant by providing a constant source of oxygen for

the cells.[22,23] The scaffold is first implanted into the host without the transplant cells, and blood vessels are allowed to infiltrate and grow into the gaps.[22] The cells are then be transplanted after a certain level of vascularization is reached.[22,23] This process will ensure that there is always be an oxygen supply close to the cells.[22] The ability to measure oxygen levels non-invasively, and thereby repeatedly, is essential for understanding the vascularization process in the scaffold over time and determining the appropriate amount of time needed for the pre-vascularization process.

Chapter 2: Exponential Decay System

2.1 Introduction

There have been previous tissue engineering attempts to cure T1D. Macroencapsulation methods have been of interest due to their ability to protect transplanted islets from the host's immune response, but most attempts have been unable to allow adequate diffusion of resources for cell survival.[19] Kidney capsules had shown potential as a possible site of transplantation due to a study in which rats with kidney subcapsular islet transplants were able to achieve normoglycemia and normal insulin levels.[25] However, the results are not translatable to humans since human kidneys have a relatively poor blood supply to support the islet transplants and there is not enough viable space for the kidney grafts.[26] Recent studies have been exploring the feasibility of islet transplantations in other regions of the body, such as skeletal muscle sites, the liver, or subcutaneous spaces.[22,25,26] The subcutaneous space is particularly appealing since it allows for easy accessibility and monitoring of the implant and islets.[22,25]

Oxygen is critical for the successful transplantation of islet cells. As shown by previous studies, sufficient oxygen prevents cell necrosis and increases insulin secretion.[27] Many optical oxygen techniques have been developed for bio applications, which can be classified as intensity-dependent or lifetime-dependent methods.[28] Intensity-based signal can be influenced by many external factors, such as skin thickness, outside light, skin color, and angle of measurements, and may be unreliable.[29] Luminescence lifetimes are intrinsic properties of lumiphores.[28] After a lumiphore is excited by absorbing a photon, it can return to ground state via phosphorescence emissions in the presence of a heavy atom, such as platinum.[28] The presence of oxygen quenches this process and is concentration and diffusion

limited.[28] Lifetime-based oxygen methods offer more robust and accurate measurements that are independent of external factors.

In this study, the vascularization trends of PDMS islet scaffolds implanted in the subcutaneous space of mice are observed using an optical oxygen sensing system. The following described experiments were run in collaborations with Dr. Avid Najdahmadi and Rachel Gurlin.

2.2 Materials and Methods

2.2.1 PDMS Device Fabrication

PDMS (Sylgard® 184 Silicone Elastomer Kit, Dow Corning Corp., Midland, MI, USA) devices were fabricated within printed 3D molds as previously described by Gurlin *et al.*[22] Molds were designed in SolidWorks (Dassault Systemes Solidworks Corp., Waltham, MA, USA) and printed with a high resolution stereolithography 3D printer (Pico Plus 27, Asiga, Anaheim Hills, CA, USA) using hard 405-nm light curable resin (PlasGRAY, Asiga). Each mold was fabricated layer-by-layer in 25-µm-thick slices. To remove any uncured resin, the molds were washed three times in isopropanol and sonicated for 10 minutes in isopropanol. After air drying for 15 minutes, the molds were further cured by 10 min exposure to an 8W 302 nm UV light source (Dual UV Transilluminator, VWR International, Radnor, PA, USA) and baked in an oven overnight at 80°C. Liquid PDMS (1:10 ratio of crosslinker to monomer base) was poured into the molds and cured at 80°C for 2 hours. The polymerized devices were removed from the molds and attached to a flat PDMS sheet after plasma treatment (Harrick Plasma, Ithaca, NY, USA). Slits in the bottom sheet were cut out using the slits from the bonded piece as a guide.

Each fabricated PDMS device had overall approximate dimensions of 10mm x 13mm x 1.2mm and contained a parallel array of four slits with widths of 500μm, three channels with inner diameters of 700μm, and windows connecting the slits and channels, which were 100μm in height and 750μm in width. The walls between each of the slits and channels were 600μm wide.

2.2.2 Oxygen Sensitive Tube (OST) Fabrication

OSTs comprise of oxygen-sensitive dye that is coated on the inner wall of a biocompatible, oxygen-permeable silicone tube. The oxygen-sensitive dye, platinum (II)-meso-tetra (4-fluorophenyl) tetrabenzoporphyrin (PtTPTBPF), has peak absorptions at 430 and 614nm and peak emission at 733nm (Frontier Scientific, Logan). The dye was mixed with polystyrene (MW 2500, Sigma, St. Louis, USA) and dissolved in chloroform (Sigma, St. Louis, USA) at a 1:15:225 ratio of dye to polystyrene to chloroform. The dye solution was flushed through silicone tubes (BTSIL_047, Instech Laboratories, USA) five times to form homogeneous coats of PtTPTBPF dye along the inner tube walls. The oxygen-permeable silicone tubes had inner and outer diameters of 0.51mm and 0.94mm, respectively. The coated tubes were stored for 24 hours in a dark, well-ventilated environment at 24℃ to allow the chloroform to evaporate. To increase mechanical stability, 24-gauge stainless-steel wires (Kanthal A1, Sandvik, Sweden) were inserted into each tube. The tubes containing wires were cut into 12-15mm sections to match the length of the PDMS devices. Finally, the ends of each tube segment were sealed with medical grade silicone adhesive (MED-1000 Nusil, USA) and the OSTs were cured at room temperature in a dark environment for two days. One OST was placed into each channel of the PDMS devices, and the fully assembled devices were sterilized in 70% alcohol for 12 hours.

2.2.3 Oxygen Monitor

The oxygen monitor was fabricated as previously described by Weidling *et al* and measures the phosphorescence emission of the oxygen sensitive dye.[30] The monitor consists of a custom printed circuit board (PCB) that houses a silicon photodetector (FDS100, Thorlabs, USA) and two red light emitting diodes (LEDs) that have central emission wavelengths of 617 nm (Luxeon Rebel, Lumileds, Netherlands). The oxygen monitor sits on the surface of the skin, excites the implanted OSTs by flashing light through the skin, and records luminesce emission waveforms. An optical bandpass filter that only passes infrared wavelengths was used to filter excitation wavelengths and allow only the dye emission wavelengths to pass. For each measurement, both LEDs were flashed simultaneously 25 times at 1% duty cycle (100μs on, 10200μs off) to excite the oxygen sensitive dye, and the emissions were passed through the optical filter onto the photodiode. The electrical current of the photodiode was converted to voltage by an operational amplifier and sampled over a period of 200 microseconds at a frequency of 500 kHz with a myRIO Data Acquisition Module (National Instruments, USA). The data acquisition timing was controlled by a LabVIEW 2015 code (National Instruments, Austin).

2.2.4 OST Calibration

The OSTs were calibrated in a resealable glass chamber with inlet and outlet ports to allow controlled gas flow. An OST was placed individually inside the chamber and the sealed chamber was placed above the oxygen monitor. 160mmHg (21%), 76mmHg (10%), 38mmHg (5%), 15.2mmHg (2%) and 0mmHg (0%) oxygen gases were flowed through the chamber, and the corresponding lifetime (τ) of each oxygen concentration was measured to generate a calibration curve. OSTs were then matched into groups of three based on their

calibration curves, inserted into the channels of the PDMS devices, and recalibrated to determine the overall calibration curve of the device.

2.2.5 Animal Study

All described animal procedures were approved by the University of California Institutional Animal Care and Use Committee at the University of Irvine (IACUC # 2008-2850). PDMS devices were implanted in the subcutaneous space of eight-week old male athymic nude mice (n=5) for eight weeks. The animals were housed at a University of California, Irvine animal facility and maintained under 12-hour light/dark cycles with *ad libitum* access to water and standard chow. Animals were monitored daily until the devices were explanted.

2.2.6 Dynamic Inhaled Gas Test (DIGT)

To monitor the vascularization process *in vivo* over an eight-week period, DIGT measurements were performed on mice with implanted PDMS devices at 3-, 7-, 14-, 21-, 28-, 35-, 42-, 49- and 56-day timepoints post implantation (n=5). For the DIGT measurements, each mouse was anesthetized while breathing 760 mmHg (100%) oxygen with 2-3% of isoflurane (Piramel Healthcare, Morpeth, United Kingdom). After the animal was under full anesthesia, the gas was changed to 152mmHg (21%) oxygen with 1.5% isoflurane. The oxygen monitor was placed on the skin of the mouse directly above the implanted PDMS device. After 100 measurements (spaced by 4.25s for a total of 425s), the inhaled oxygen was switch back to 760mmHg.

The tissue PO_2 is expected to rise and fall as the inhaled PO_2 is increased and decreased, respectively, and reach a plateau when a certain oxygen concentration is breathed for an extended period of time. Once the measured lifetimes plateaued after switching back to

760mmHg oxygen, animals were taken off of anesthesia and returned to cages. The time to plateau is calculated using a MATLAB (MathWorks, Natick, MA, USA) code and reported as the *Risetime*.

2.2.7 Conversion from Lifetime to PO_2

The measured voltages from the photodiode were converted to emission decay lifetimes and then to oxygen concentrations with a MATLAB code. The oxygen sensitive dye emits photons after each excitation that are detected by the photodiode and recorded as a voltage. The relationship between the voltage readings and lifetime values can be modeled with the exponential function:

$$V = V_0 e^{(\frac{-t}{\tau})}$$

Where V is the detector voltage, V_0 is the voltage at the start of the decay, t is the time in seconds after LED excitation, and τ is the lifetime reported in seconds.[30] The lifetime values were computed using a nonlinear least squares regression curve fit.

To determine the calibration curve for the individual or grouped devices, the average lifetimes (τ) of 25 cycles were used. Oxygen quenches the emissions of the excited porphyrin dye, which results in lifetimes (τ) decreasing with increasing PO_2.[28] Although the mechanism in which the oxygen quenches the dye is not completely clear, the kinetics of quenching is described by the equation:

$$1 - \frac{\tau}{\tau_0} = k \cdot pO_2$$

Where τ and τ_0 are the lifetimes the phosphorescent decay of luminophore in the presence and absence of the quencher, and k is the quenching constant.[28] Using the quenching

constant, k, determined for each PDMS device, the measured lifetimes from both the *in vitro* calibrations and the *in vivo* animal experiments can be converted to PO_2.

2.2.8 Histological Analysis and Immunofluorescence Staining

PDMS devices were removed 56 days (8 weeks) after implantation by cutting through the surrounding skin and leaving the tissue above and below the device intact. The excised tissues were immediately fixed in a 4% solution of phosphate-buffered formalin for 24h. Samples were embedded in paraffin, sectioned vertically, and stained with hematoxylin and eosin (H&E) (JIT Labs, Irvine, CA, USA). For immunohistochemistry, sections were deparaffinized followed by antigen retrieval via overnight incubation in 0.1 M Tris/HCl buffer, pH=9.0 at 80°C. Sections were then washed with phosphate-buffered saline (PBS), permeabilized with 0.5% Triton X-100, and blocked with 5% Donkey serum (Jackson ImmunoResearch, Inc., West Grove, PA, USA) for 30 minutes at room temperature. After serum blocking, slides were incubated with 1:200 monoclonal rabbit anti-alpha smooth muscle actin (αSMA) (Abcam, Cambridge, MA, USA) and 1:200 polyclonal goat anti-CD31/PECAM-1 (sc-1506, Santa Cruz Biotechnology, Santa Cruz, CA, USA) in 1x PBS supplemented with 5% Donkey serum and 0.5% Triton X-100 at 4°C overnight. Slides were then washed with PBS and incubated with 1:500 AlexaFluor® 488 donkey anti-rabbit (Life Technologies, Carlsbad, CA, USA) and 1:400 AlexaFluor® 594 donkey anti-goat (Jackson ImmunoResearch, Inc. West Grove, PA, USA). Images were taken on an Olympus IX83 microscope at 20x with an Orca R2 camera (Hamamatsu Photonics K.K., Hamamatsu City, Japan) through Micro-Manager and stitched together using FIJI.

2.2.9 Statistics

Statistical analyses were performed in GraphPad Prism (version 7.0d; GraphPad Software, Inc., La Jolla, USA) and MATLAB. One-way ANOVA and student t-tests were used to evaluate the data. P-values less than 0.05 were considered significant. The data is presented in mean ± standard deviation.

2.3 Results

The OSTs were individually calibrated at the different oxygen levels previously mentioned in Section 2.2.4 and matched in groups of three according their calibration curves. Figure 2.1A shows a matched group after it has been inserted into a PDMS device. Each device is recalibrated at the various oxygen levels in stepwise intervals (Figure 2.1B), and the mathematical relationship between average lifetime values (τ) and PO_2 is modeled (Figure 2.1C). The original stepwise calibrations of the matched groups are converted to PO_2 to verify the accuracy of the transformation functions (Figure 2.1D).

A)

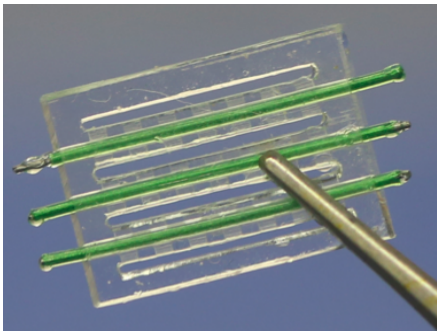

B)

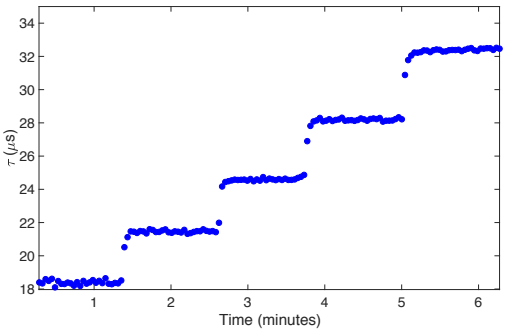

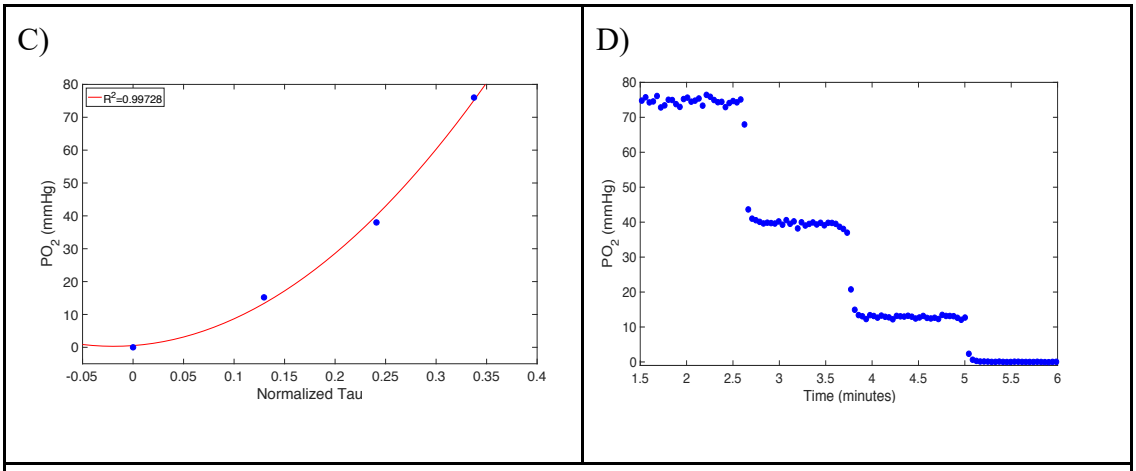

Figure 2.1 Calibration of PDMS devices with OSTs prior to implantation. (A) Three OSTs with matching lifetime calibration curves are inserted into the channels of PDMS devices. (B) PDMS devices are calibrated in step-wise PO_2 concentration intervals inside a sealed gas chamber and the corresponding τ values are measured. (C) The mathematical relationship between τ and PO_2 is modeled using the average τ at each concentration. (D) The original calibration curve is converted to PO_2 based on the mathematical model to validate the conversion function.

Both fluorescence emission intensities and phosphorescence emission decays are characteristics of porphyrin dyes used for oxygen sensing.[28] Lifetime emission decays are preferable to intensity measurements because the scattering of light when passing through the PDMS devices and their surrounding tissue or the possible misalignments of the oxygen probe over the skin of animal could cause changes in the signal intensities and result in inaccurate PO_2 measurements. To validate that our chosen phosphorescent approach is independent of signal intensity, a PDMS device with OSTs is gradually displaced in the x direction (parallel to length of OST) from the center of the oxygen monitor at 2mm increments. Figure 2.2 shows that despite decreasing signal intensity as the horizontal displacement increases, the lifetime values remained constant for up to 10mm of misalignment, which is close to the length of the OSTs.

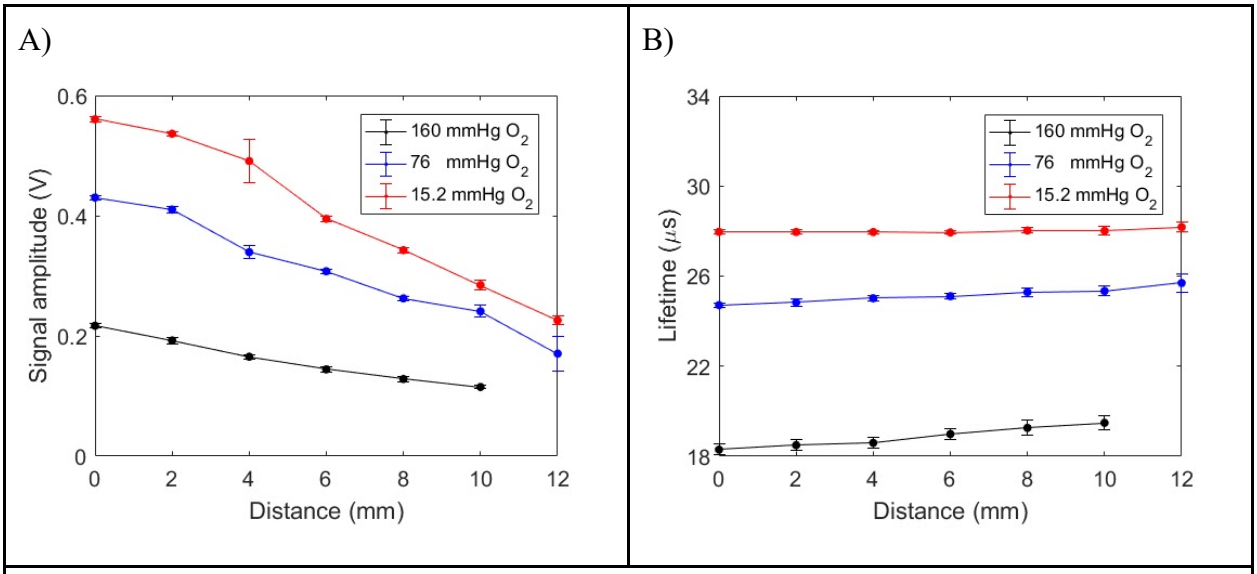

Figure 2.2 Lifetime (τ) values are independent of signal intensity. Movement of the probe from the center of the OSTs at 160mmHg, 76mmHg, and 15.2mmHg oxygen shows (A) the signal intensities reduce as distance increases; however, (B) the calculated average τ values remain relatively constant despite distance. This experiment validates the strategy of using emission lifetime decay instead of signal intensity for monitoring oxygen tension in vivo.

After implantation, DIGT measurements were performed on the days specified in 2.2.6. The measured lifetimes were converted to PO_2 with the corresponding transformation models for the implanted PDMS devices (Figure 2.3A). The *Risetime*, or time period corresponding from when the animals were switched back to 760mmHg oxygen until the oxygen dynamics reached a plateau, were analyzed for each animal. The slopes of the *Risetimes* were used as a metric of comparison over the duration of the experiment and represent the rate of oxygen dynamics *in vivo* in response to the changes in oxygen concentrations inhaled. The slope measurements across all nine timepoints are shown in Figure 2.3B. The slopes during the first two weeks were significantly higher than that of the later timepoints. A select few statistics are shown in Figure 2.3C that is representative of the overall significance trends in the data.

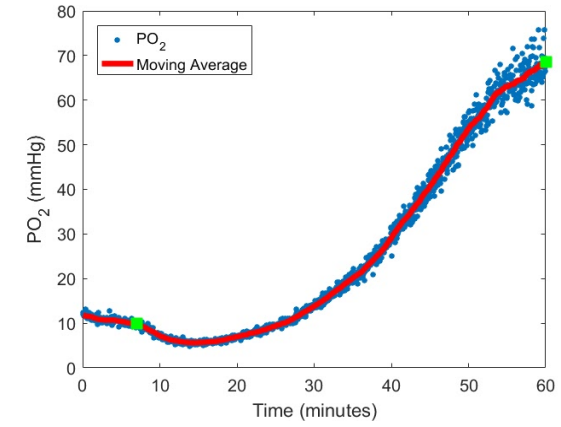

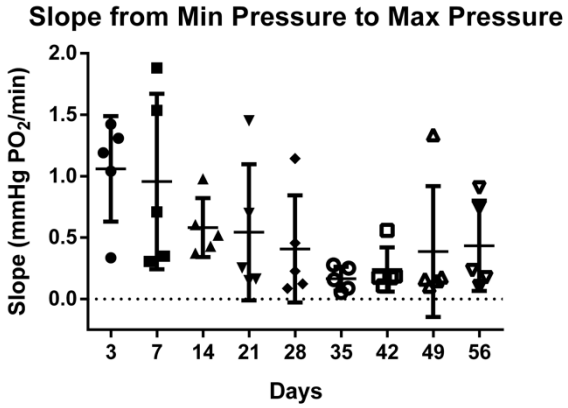

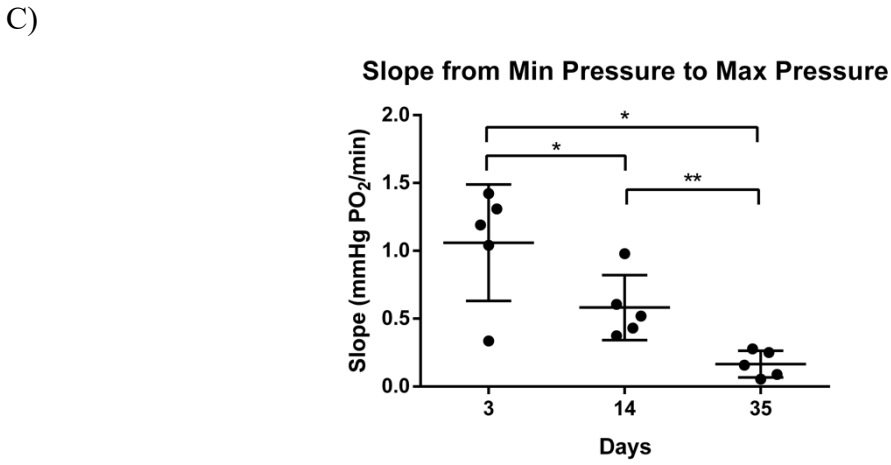

Figure 2.3 Comparison of *Risetime* slopes across eight weeks. (A) DIGT tests after conversion of τ values to PO_2 show increases in device oxygenation. The green boxes indicate the period in which the animal is breathing 760 mmHg, and the elapsed time in this period is defined as *Risetime.* (B) Slopes of the *Risetime* were calculated. The slope corresponds to the response rate of oxygen changes at the islet transplantation site to the changes in oxygen concentrations inhaled. Each data point represents a single DIGT test. (C) A select few timepoints and statistics representative of the trend from all the data points shows decreasing slope values until day 35.
* = $p<0.1$, ** = $p<0.01$.

The PDMS devices were explanted after 56 days. The excised devices and surrounding tissues were sectioned vertically, as shown in Figure 2.4A. Immunostaining for CD31 and αSMA confirmed the presence of new vasculature inside the devices (Figure 2.4B and 2.4C), and the quantified vessel counts showed similar values for all of the mice (Figure 2.4D).

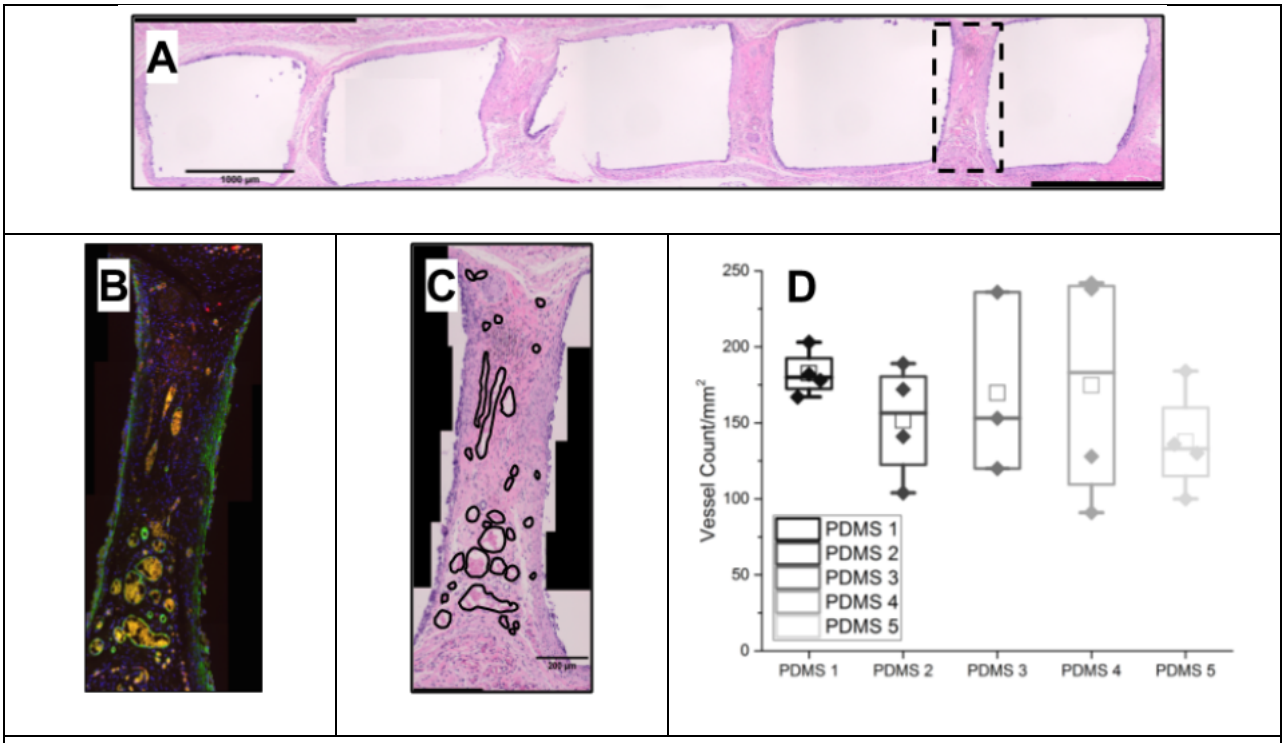

Figure 2.4 Histology results of slit tissue within PDMS devices after eight weeks of implantation. (A) H&E staining of a vertical view of the opening tissue surrounding the device. (B) A zoomed in view of immunostaining of the same opening tissue for αSMA (green) and CD31 (red) shows a vascularized area. (C) Black outlines were hand drawn on H&E images to get vessel counts per slit area. (D) Quantification of vessel count within the openings tissue of PDMS devices. The vessel count for all five devices showed similar values that were not significantly different from each other (p=0.7).

2.4 Discussion

Tissue engineering is a promising cure to T1D that would alleviate or cease patient reliance on daily insulin injections or immunosuppressants.[19] The ultimate success of the tissue scaffold depends on its ability to transfer enough oxygen and nutrients from the host to survive.[18,19,21,25] Sufficient oxygen levels, in particular, have been shown to increase insulin secretion and reduce the number of islets needed for diabetes reversal, thereby increasing the effectiveness of the transplant.[27] Having a constant viable oxygen source, however, has been one of the greatest challenges to overcome for current tissue engineering attempts.[18,19,21,25] The tissue implant can trigger a series of foreign body responses, such as granulation tissue development, chronic inflammation, and fibrosis and fibrotic capsule formation, that limit the

oxygen diffusion capabilities and render the scaffold futile.[18–20,25,31] Pre-vascularization has shown potential for overcoming the lack of oxygen within the scaffold, but the optimal time duration for the process has not yet been fully explored.[18,22,25,27] Measuring oxygen dynamics within the scaffold over time may provide insight on the angiogenesis process and the foreign body reaction due to the direct correlation between the amount and distance of vasculature and oxygen diffusion rates.

In this study, we demonstrated a robust technique to measure the changes of oxygen dynamics in an implanted PDMS-based scaffold over an eight-week period. Using the phosphorescent emission properties of a porphyrin dye, oxygen at the exact site of islet transplant within the scaffold was quantified and tracked non-invasively. This provides a clue of the host response to the scaffold and its potential as a viable tissue engineering solution for islet transplants.

The slope of the *Risetime*, which corresponds the response rate of oxygen dynamics at the islet transplantation site to the changes in oxygen concentrations inhaled, showed significant difference between measurements taken in the first two weeks after implant and the later timepoints. This can possibly be explained as the wound healing effects around the site of implantation. The inflammation time for healthy wound healing is around one to two weeks, which falls in line with the observed measurements.[32] Angiogenesis during wound healing is often correlated with inflammation due to the large amounts of proangiogenic mediators produced by the inflammatory cells.[31–33] It has been shown that as the inflammation reduces, there is selective regression of the newly formed capillary beds, which have many more capillaries than normal tissue, into a vascular density that is similar to the density of normal tissue.[33] Due to the increase in vasculature in the time period following the surgery, the

oxygen dynamics local to the site of implant are more responsive and adjust faster to the inhaled oxygen concentrations than under normal conditions. As the wound heals and the capillaries regress, the response rate decreases.

While histology showed new vasculature present in the devices, there was no significant difference in oxygen dynamics amongst the later timepoints after the initial wound healing phase. However, a trend can be observed where the oxygen diffusion measurements reach a plateau and then increase slightly. This slight increase may correspond to beginning of angiogenesis and growth of the observed new vasculature. The lack of statistical significance may be due to the extent of vascularization being too low to produce a measurable difference in oxygen diffusion rates. This is further corroborated with the statistically higher slope values of day 14 than the slopes of day 35 but not day 56, which suggests that the oxygen diffusion rates and amount of vasculature present at day 56 may be comparable with the that of the end of the inflammation and wound healing stage. In previous studies, we had shown that scaffolds with similar designs and the same PDMS material as the one used in this study were shown to have varying amounts of angiogenesis and new tissue growth based on the width and geometry of the slits.[22] This coupled with evidence that morphological features also affect the foreign body response of the scaffold may suggest the dimensions and geometries used in these devices were not optimal for efficient angiogenesis or the time duration of the experiment was not long enough for sufficient vasculature growth.[20] Further studies with longer timepoints are still needed to confirm this theory.

In summary, the results of this study show that we are able to track changes in oxygen dynamicss in our device non-invasively, and that our scaffold design has potential for islet transplantation; however, the exact host responses to our tissue scaffold over time is still

unclear. The scaffold promoted angiogenesis, which is corroborated by previous studies with the same material and similar designs, but the vessel count may still be too low for islet survival. This may indicate that the size and geometry of the scaffold may play a role in the vascularization process. An important feature of our oxygen detection system and tissue scaffold is that they are able to yield results independent of pharmaceutical factors, which is preferable for both regulatory agencies and patient use.

Chapter 3: Phasor System

3.1 Introduction

While exponential decay systems offer reliable, robust oxygen concentration measurements independent of intensity, they usually demand complicated and expensive instrumentation due to the need for high speed data acquisition, fast pulsing LEDs, and specific signal processing systems.[29] All instrumentation in exponential decay systems must operate at a timescale of microseconds to capture the lifetime decay of the oxygen sensitive dye.[28,29] Additionally, as seen in our system, the low signal to electrical noise ratio as the emission signal drops off after each excitation may cause bias and inaccuracies in the measurements.

Optical oxygen sensing based on phase shift detection overcomes these concerns. Instead of excitation with a square pulse as in the exponential decay method, the phasor system excites oxygen sensitive dye with a sinusoidally-modulated light at a fixed frequency, which produces a sinusoidal emission signal with the same frequency.[29] Similar as described in Chapter 2, the emission of the oxygen sensitive dye is quenched at varying degrees by the presence of different concentrations of oxygen.[28] The measured phase shifts between the excitation and emission signals correspond with lifetimes values that can be converted to PO_2.[29] Fewer sampling points are needed to accurately characterize a wave function than an exponential function, so cheaper instrumentation with lower processing powers can be used.[29,34] While electrical noise in the system may shift the amplitude of the signal captured, it does not affect the phase of the wave. Therefore, the system is robust to any electrical noise and variance in signal intensity.

In this study, a phasor system was designed and built to improve the current optical oxygen sensing technique used for islet transplant studies. The described integrating circuits and operational system codes were made in collaboration with Dr. Mark Keating.

3.2 Materials and Methods

3.2.3 Oxygen Sensitive Tube (OST) Fabrication

OSTs comprise of oxygen-sensitive dye that is coated on the inner wall of a biocompatible, oxygen-permeable silicone tube. The oxygen-sensitive dye, platinum (II)-meso-tetra (4-fluorophenyl) tetrabenzoporphyrin (PtTPTBPF), has peak absorptions at 430 and 614nm and peak emission at 733nm (Frontier Scientific, Logan). The dye was mixed with polystyrene (MW 2500, Sigma, St. Louis, USA) and dissolved in chloroform (Sigma, St. Louis, USA) at a 1:15:225 ratio of dye to polystyrene to chloroform. The dye solution was flushed through silicone tubes (BTSIL_047, Instech Laboratories, USA) five times to form homogeneous coats of PtTPTBPF dye along the inner tube walls. The oxygen-permeable silicone tubes had inner and outer diameters of 0.51mm and 0.94mm, respectively. The coated tubes were stored for 24 hours in a dark, well-ventilated environment at 24℃ to allow the chloroform to evaporate. To increase mechanical stability, 24-gauge stainless-steel wires (Kanthal A1, Sandvik, Sweden) were inserted into each tube. The tubes containing wires were cut into 12-15mm sections. Finally, the ends of each tube segment were sealed with medical grade silicone adhesive (MED-1000 Nusil, USA) and the OSTs were cured at room temperature in a dark environment for two days.

3.2.2 Oxygen Monitor

Similar to the oxygen monitor for the exponential decay system, the oxygen monitor for the phasor system is a sensor placed on the surface of the skin that measures the

phosphorescence emissions of the oxygen sensitive dye through a photodiode (S6775-01, Hamamatsu Photonics, Japan). Integrating circuits (ICs) with different operational amplifiers (op-amps) and LEDs were designed in EAGLE (Autodesk, USA) and printed on a printed circuit board (PCB). The two different op-amps tested were the LTC6244 (Linear Technology, USA) and the AD8065 (Analog Devices, USA). The LTC6244 is a dual op-amp, while the AD8065 is a single. The two LEDs compared were the Luxeon Red-Orange Rebel LED (Lumileds, Netherlands) and the Kingbright SMD Orange Chip LED (Kingbright Company, USA). The emission wavelengths for the LEDs were centered around 617nm and 605nm, respectively. Components were soldered on using solder paste (SMD291SNL, Chip Quik, Canada) and a hot plate. The resulting ICs were compared, and the best op-amp – LED combination was optimized for the phasor oxygen detection system for future possible *in vivo* applications.

The LEDs were sinusoidally modulated at a frequency of 10 kHz, and the porphyrin dye emissions were sampled at 20 kHz with a myDAQ (National Instruments, USA). The data acquisition was controlled by a LabVIEW 2015 (National Instruments, Austin) code, and the phase shift between the excitation and emission signals were recorded.

3.2.3 OST Calibration

The OSTs were calibrated in a resealable glass chamber with inlet and outlet ports to allow controlled gas flow. An OST was placed individually inside the chamber and the sealed chamber was placed above the oxygen monitor. 160mmHg (21%), 76mmHg (10%), 38mmHg (5%), 15.2mmHg (2%) and 0mmHg (0%) oxygen gases were flowed through the chamber, and the corresponding phase shift of each oxygen concentration with regards to the excitation signal was measured to generate a calibration curve.

3.2.4 Conversion from Phase Shift to PO_2

The measured phase shifts from the photodiode were converted to emission lifetimes and then to oxygen concentrations with a MATLAB (MathWorks, USA) code. The oxygen sensitive dye emits photons after each excitation in a sinusoidal pattern with the same frequency as the excitation signal. The emission signal is detected and recorded by the photodiode and the phase is extracted. The relationship between the phase shift and lifetime values can be modeled with the function:

$$\tan(\theta) = (2\pi f) \cdot \tau$$

Where θ is the phase shift between the excitation and emission signals, f is the frequency of the signals, and τ is the lifetime reported in seconds.[29] All phase shifts were converted to lifetimes for further data processing.

To determine the calibration curve, the average lifetimes (τ) of 20 cycles were used. Oxygen quenches the emissions of the excited porphyrin dye, which results in lifetimes (τ) decreasing with increasing PO_2.[28] Although the mechanism in which the oxygen quenches the dye is not completely clear, the kinetics of quenching is described by the Stern-Volmer equation:

$$\frac{\tau_0}{\tau} - 1 = k \cdot pO_2$$

Where τ and τ_0 are the lifetimes the phosphorescent decay of luminophore in the presence and absence of the oxygen quencher, and k is the quenching constant.[28] The quenching constant, k, is unique for each type of dye, and needs to be calculated for different applications. Using the quenching constants, the measured lifetimes from the calibrations are converted to PO_2 to verify the accuracy of the transformation functions.

3.3 Results and Discussion

3.3.1 Phasor System Integrating Circuit (IC)

Op-amps amplify the detected porphyrin dye emission signals to a measurable range for the data acquisition system. The ICs compared were primarily designed based on the suggested circuitries described in the data sheet for the single and dual op-amps, as shown in Figure 3.1A and 3.1B, respectively.[35,36] The single op-amp has a simple circuit that involves only capacitors and resistors to control the feedback loop of the op-amp, while the dual op-amp also has a JFET drain gate to bootstrap the capacitance.

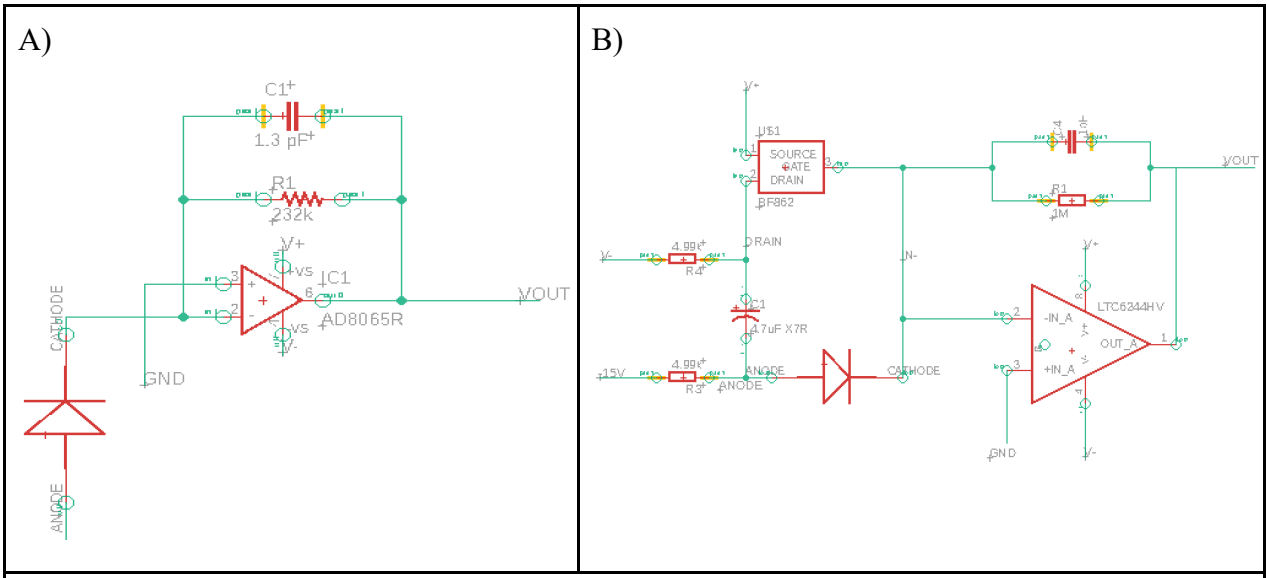

Figure 3.1 IC schematics of the photodiode and op-amps. (A) The single op-amp only uses capacitors and resistors for the feedback loop. (B) The dual op-amp uses both a system of capacitors and resistors and a JFET drain gate to control the feedback of the op-amp.

LEDs are used to excite the porphyrin dye.[28] The dye used for our experiments has peak absorptions at 430nm and 614nm, and peak emission at 733nm.[37] Although the red-orange LED has a 617nm emission wavelength that is closer to the peak absorption of the dye, this

wavelength crosses into the spectral response range of the photodiode and may interfere with emission detections.[38,39] An infrared bandpass filter is needed to limit the bleed over from the red-orange excitation signal and only allow the emission wavelengths to pass to the photodiode. The orange LED is able to achieve similar results without the filter since its wavelength has minimal overlap with the spectral response of the photodiode.[39,40] However, the red-orange LED has a higher power and larger viewing angle (90mW; 125°) than the orange LED (75mW, 120°), which can be used to penetrate through skin and excite the dye during *in vivo* measurements better.[38,40]

3.3.2 IC Comparison and Application

The different op-amp and LED combinations were compared by calibrating the same OSTs in the oxygen concentrations mentioned in Section 3.2.3. From the results, it was determined that the IC with the dual op-amp and red-orange LED produced the strongest signal with the least amount of signal noise. This may be due to the larger gain from the dual op-amp and the stronger excitation and emission signals produced by the higher-powered LEDs. A sample OST calibration curve using the phasor system, the mathematical relationship between lifetime and PO_2, and the converted PO_2 values are shown in Figure 3.2A-C to demonstrate the efficiency of this system.

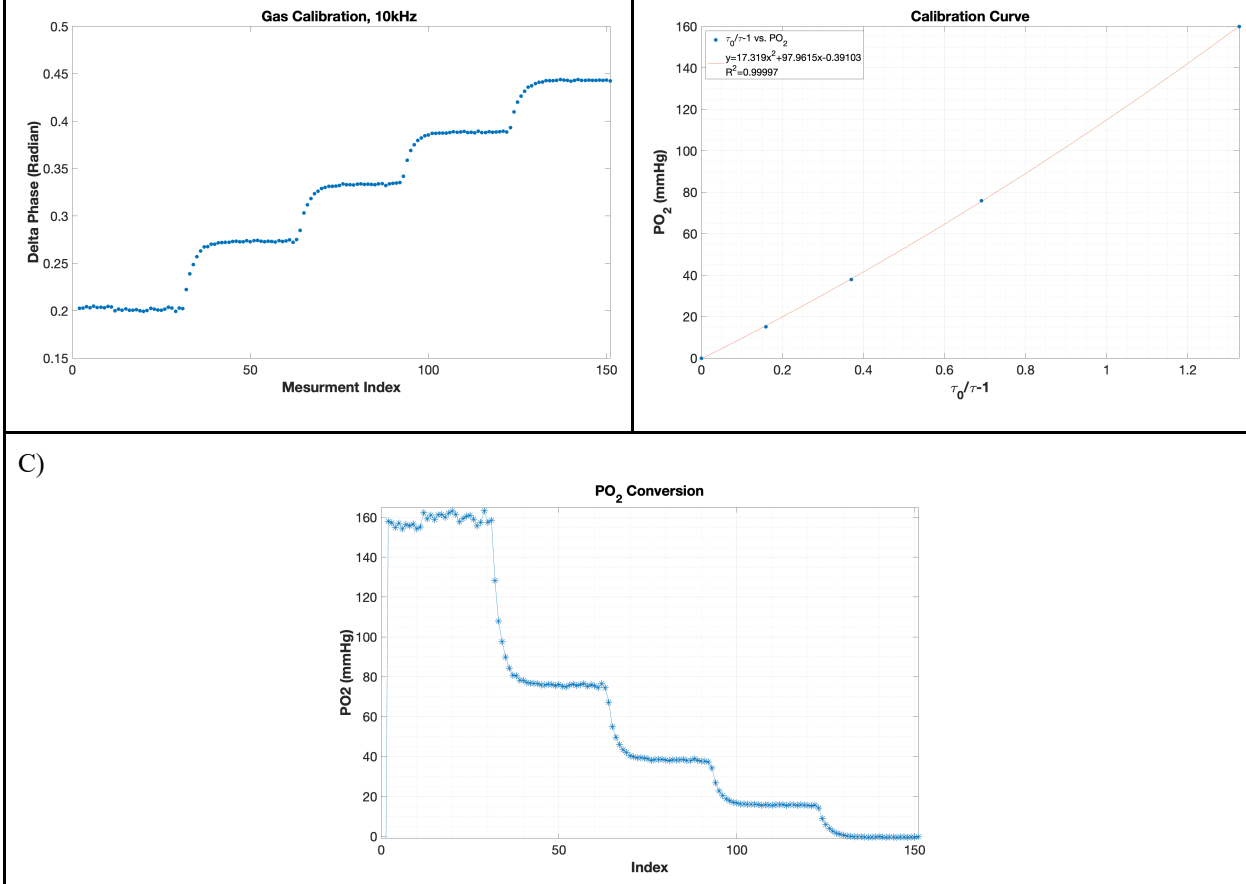

Figure 3.2 Calibration of OSTs using phasor oxygen sensing. (A) An OST is calibrated in step-wise PO_2 concentration intervals inside a sealed gas chamber and the corresponding phase shifts (θ) are measured. (B) After conversion from θ to τ, the mathematical relationship between τ and PO_2 is modeled using the average τ at each concentration. (C) The original calibration curve is converted to PO_2 based on the mathematical model to validate the conversion function.

3.4 Conclusion

Optical sensing based on phase-shift detection offers robust oxygen measurements without the need for high speed instrumentation and high processing powers. Wave features can be characterized with fewer sampling points than exponential functions, which allows for reliable measurements that are less sensitive to electrical noise and external factors. In this chapter, we developed a phasor optical oxygen sensing system that can measure oxygen

concentrations and diffusion rates with more accuracy than the previous exponential decay method. This system can be used for future *in* vivo tissue scaffold transplant studies and detection of smaller devices and OSTs, which could drive further improvements towards successful tissue engineering cell therapy.

Chapter 4: Summary and Future Work

The efficient delivery of oxygen to the transplanted islets is critical for the success of the tissue scaffold. Although there have been many material and design innovations that have improved angiogenesis and the survival of islets, there is still no method that can consistently overcome the challenge and allow for prolonged islet survival and insulin secretion. Pre-vascularization of the scaffold is an approach that may improve success of the implant by providing a closer source of metabolic transport for the cells.

In the first chapter, we demonstrated a technique to optically measure oxygen concentrations non-invasively in a subcutaneously implanted PDMS-based tissue scaffold over eight weeks. Tracking oxygen dynamic at the site of islet transplantation over time may provide insight into the vascularization process and the foreign body response to the scaffold. While the results showed an increase in oxygen diffusion rates during the initial wound healing stage, there was no statistical difference at the later timepoints despite the presence of new vasculature. The exact mechanics of this process are not clearly understood and requires further studies and elucidation. To measure oxygen more accurately, in the second chapter, we developed a more robust optical oxygen sensor that uses the phase-shift between the sinusoidally modulated excitation and emission signals instead of exponential lifetime decay. Fewer sampling points are needed to accurately characterize a wave function than an

exponential function, which yields more robust measurements. This new sensor reduced the required processing power of the instrumentation and provided more reliable measurements even for low signals.

Further studies with more animals and different techniques, such as lectin perfusion or second harmonic generation imaging, are needed to better understand the vascularization and foreign body response of the implant. It would be informative to correlate histology at each timepoint with the measured oxygen partial pressures. Measuring the oxygen dynamics of scaffolds that have shown high amounts of vascularization and comparing the results to our scaffold could also provide insight to the advantages and disadvantages of the different designs and materials used. The results could be applied to further improve the mass transfer rates and immune protection capabilities of the scaffolds. Other materials, such as bicontinuos interfacially jammed emulsion gels (bijels), may also be considered to replace the PDMS material due to their limited foreign body responses. Since size of the implant has been shown to play a role in the wound healing, smaller scaffolds and OSTs may be explored. The development of the phasor oxygen sensing system enables reliable oxygen measurements at low signal from the smaller OSTs without the interference of electrical noise.

References

1. (CDC), C. for D. C. and P. Centers for Disease Control and Prevention. National Diabetes Statistic Report:Estimates of Diabetes and Its Burden in the United States,2014. *Reporteros Sin Front.* 2009–2012 (2013).

2. Imperatore, G. *et al.* Projections of type 1 and type 2 diabetes burden in the U.S. population aged <20 years through 2050: Dynamic modeling of incidence, mortality, and population growth. *Diabetes Care* **35**, 2515–2520 (2012).

3. L.A., D., C., E.-M. & R.A., O. Type 1 diabetes. *Lancet* **391**, 2449–2462 (2018).

4. Foster, N. C. *et al.* State of Type 1 Diabetes Management and Outcomes from the T1D Exchange in 2016–2018. *Diabetes Technol. Ther.* **21**, 66–72 (2019).

5. Beck, R. W. *et al.* The T1D exchange clinic registry. *J. Clin. Endocrinol. Metab.* **97**, 4383–4389 (2012).

6. Farabi, S. S. Type 1 diabetes and sleep. *Diabetes Spectr.* **29**, 10–13 (2016).

7. Colberg, S. R., Laan, R., Dassau, E. & Kerr, D. Physical activity and type 1 diabetes: Time for a rewire? *J. Diabetes Sci. Technol.* **9**, 609–618 (2015).

8. Heinemann, L. Finger pricking and pain: A never ending story. *J. Diabetes Sci. Technol.* **2**, 919–921 (2008).

9. Miller, K. M. *et al.* Current state of type 1 diabetes treatment in the U.S.: Updated data from the t1d exchange clinic registry. *Diabetes Care* **38**, 971–978 (2015).

10. Bergenstal, R. M. *et al.* Effectiveness of Sensor-Augmented Insulin-Pump Therapy in Type 1 Diabetes. *N. Engl. J. Med.* **359**, 1543–1554 (2008).

11. Ovalle, F. Continuous Glucose Monitoring and Intensive Treatment of Type 1 Diabetes. *Yearb. Endocrinol.* **2009**, 34–35 (2012).

12. Stratta, R. J., Fridell, J. A., Gruessner, A. C., Odorico, J. S. & Gruessner, R. W. G. Pancreas transplantation: A decade of decline. *Current Opinion in Organ Transplantation* (2016). doi:10.1097/MOT.0000000000000319

13. White, S. A., Shaw, J. A. & Sutherland, D. E. R. Pancreas transplantation. *Lancet* **373**, 1808–17 (2009).

14. Knight, S., Vogel, T. & Friend, P. Pancreas transplantation. *Surg. (United Kingdom)* **35**, 397–403 (2017).

15. Dholakia, S. *et al.* Pancreas Transplantation: Past, Present, Future. *Am. J. Med.* **129**, 667–673 (2016).

16. Vacanti, C. A. The history of tissue engineering. *J. Cell. Mol. Med.* **10**, 569–576 (2006).

17. Shapiro, A. M. J. *et al.* Islet Transplantation in Seven Patients with Type 1 Diabetes Mellitus Using a Glucocorticoid-Free Immunosuppressive Regimen. *N. Engl. J. Med.* **343**, 230–238 (2002).

18. Desai, T. & Shea, L. D. Advances in islet encapsulation technologies. *Nat. Rev. Drug Discov.* **16**, 338–350 (2017).

19. Song, S. & Roy, S. Progress and challenges in macroencapsulation approaches for type 1

diabetes (T1D) treatment: Cells, biomaterials, and devices. *Biotechnol. Bioeng.* **113**, 1381–1402 (2016).

20. Akilbekova, D. & Bratlie, K. M. Quantitative Characterization of Collagen in the Fibrotic Capsule Surrounding Implanted Polymeric Microparticles through Second Harmonic Generation Imaging. 1–17 (2015). doi:10.1371/journal.pone.0130386

21. Fiedler, T. *et al.* A comparative study of oxygen diffusion in tissue engineering scaffolds. 2573–2578 (2014). doi:10.1007/s10856-014-5264-7

22. Gurlin, R. E. *et al.* Vascularization and innervation of slits within polydimethylsiloxane sheets in the subcutaneous space of athymic nude mice. *J. Tissue Eng.* **8**, 204173141769164 (2017).

23. Komatsu, H., Kandeel, F. & Mullen, Y. Impact of Oxygen on Pancreatic Islet Survival. **47**, 533–543 (2018).

24. Flood, A. B., Satinsky, V. A. & Swartz, H. M. Comparing the Effectiveness of Methods to Measure Oxygen in Tissues for Prognosis and Treatment of Cancer. *Adv Exp Med Biol.* **923**, 113–120 (2016).

25. Rajab, A. Islet transplantation: Alternative sites. *Curr. Diab. Rep.* **10**, 332–337 (2010).

26. Stokes, R. A. *et al.* Transplantation sites for human and murine islets. *Diabetologia* **60**, 1961–1971 (2017).

27. Komatsu, H. *et al.* Posttransplant oxygen inhalation improves the outcome of subcutaneous islet transplantation: A promising clinical alternative to the conventional

intrahepatic site. *Am. J. Transplant.* **18**, 832–842 (2018).

28. Quaranta, M., Borisov, S. M. & Klimant, I. Indicators for optical oxygen sensors. *Bioanal. Rev.* **4**, 115–157 (2012).

29. Chu, C., Lin, K. & Tang, Y. Sensors and Actuators B : Chemical A new optical sensor for sensing oxygen based on phase shift detection. *Sensors Actuators B. Chem.* **223**, 606–612 (2016).

30. Weidling, J., Lakey, J. R. T. & Botvinick, E. Method measuring oxygen tension and transport within subcutaneous devices. *J. Biomed. Opt.* **19**, 087006-1–5 (2014).

31. Diegelmann, R. F. & Evans, M. C. Wound healing: an overview of acute, fibrotic and delayed healing. *Front. Biosci.* **9**, 283–9 (2004).

32. Braiman-Wiksman, L., Solomonik, I., Spira, R. & Tennenbaum, T. Novel Insights into Wound Healing Sequence of Events. *Toxicol. Pathol.* **35**, 767–779 (2007).

33. DiPietro, L. A. Angiogenesis and wound repair: when enough is enough. *J. Leukoc. Biol.* **100**, 979–984 (2016).

34. Yao, L., Khan, R., Chodavarapu, V. P., Tripathi, V. S. & Bright, F. V. Sensitivity-Enhanced CMOS Phase Luminometry System Using Xerogel-Based Sensors. **3**, 304–311 (2009).

35. Analog Devices. *High Performance , 145 MHz FastFET ™ Op Amps AD8065/AD8066. D02916-0-1/19(L) datasheet* (2019).

36. Linear Technology Corporation. *LTC6244 - Dual 50MHz, Low Noise, Rail-to-Rail, CMOS*

Op Amp. *LT 1209 REV B datasheet* (2006).

37. Borisov, S. M. *et al.* New NIR-emitting complexes of platinum(II) and palladium(II) with fluorinated benzoporphyrins. *J. Photochem. Photobiol. A Chem.* **201**, 128–135 (2009).

38. Lumileds. Luxeon Rebel Color line. *DS68 LUXEON Rebel Color Line Prod. datasheet* 1–31 (2017).

39. Hamamatsu. *Standard Si PIN Photodiodes S6775 series*. *KPIN1048E06 datasheet* (2014).

40. Kingbright. APT1608CGCK 1.6 x 0.8 mm SMD Chip LED Lamp. *DSAA6059/1203001646 datasheet* 1–4 (2019).